Case Studies in Construction Materials 17 (2022) e01230

Contents lists available at ScienceDirect

Case Studies in Construction Materials

journal homepage: www.elsevier.com/locate/cscm

Experimental study effect of bottom ash and temperature of firing on the properties, microstructure and pore size distribution of clay bricks: A Lithuania point of view

Inna Pitak [a,*], Arūnas Baltušnikas [a], Regina Kalpokaitė-Dičkuvienė [a], Rita Kriukiene [a], Gintaras Denafas [a,b]

[a] Laboratory of Materials Research and Testing, Lithuanian Energy Institute, Kaunas 44403, Lithuania
[b] Department of Environmental Technology, Kaunas University of Technology, Kaunas 51424, Lithuania

ARTICLE INFO

Keywords:
Bottom ash
Recycling
Properties
Structure
Clay bricks

ABSTRACT

The paper studied the feasibility of reusing the bottom ash (BA) in clay bricks production. The study has researched the influence of BA on clay bricks' physical and mechanical properties, the micro-and structure of samples, resistance to freezing and thawing porosity, average pore size and pore size distribution. Clay bricks were made from BA from 10% to 40% and clay (with CaO less than 1%), fired at 900 and 1000 °C. The open porosity of clay bricks developed when a BA was added due to burning a small amount of organic part of clay, decarbonising calcite, and the release of gaseous substances and crystalline moisture. The infrared spectra of clay brick samples fired at 900 and 1000 °C showed the presence of Si-O, Si-O-Mg, and Si-O-Al bond. These results are consistent with the XRD patterns. Clay bricks' physical and mechanical properties changed with the presence of BA: shrinkage, density and compressive strength decreased, water absorption and open porosity increased. It is recommended to add 10% and 20% BA to the clay body and fire at 900 °C, or 10–30% BA and fire at 1000 °C. In freezing and thawing resistance, clay bricks containing BA10 and BA20 fired at 900 and 1000 °C can be utilized in moderately aggressive environments. Samples containing BA30 and fired at 1000 °C can be used in passively aggressive environments. Micropores predominate in clay bricks; however, with an increase in BA, micropores turn into mesopores. The pore diameter of samples changes with BA and the firing temperature. The specific surface area is directly proportional to the amount of added BA. The use of bottom ash in the production of clay bricks will allow producing clay brick without deteriorating its quality and reduce the consumption of natural resources by up to 30%.

1. Introduction

Many countries use the waste incineration process to generate energy. Waste that cannot recycle is sent to a cogeneration power plant (CPP) for incineration. In this case, the incineration process is considered an integral part of the waste management strategy. In waste incineration, we obtain energy, thereby saving non-renewable natural resources and reducing the amount of waste disposed of at the landfill. During the incineration process, the volume of waste is reduced by about 90%. But any technological process has

* Corresponding author.
E-mail addresses: inna.pitak@lei.lt, ipitak5@gmail.com (I. Pitak).

https://doi.org/10.1016/j.cscm.2022.e01230
Received 15 March 2022; Received in revised form 20 May 2022; Accepted 7 June 2022
Available online 10 June 2022

advantages and disadvantages. One of these disadvantages is a significant amount of BA generated due to waste incineration.

As the non-recyclable part of the waste is incinerated, the volumes of BA increase, and there is a need to develop technologies for the disposal of "new" materials [1,2].

The amount of waste generated in Lithuania is 1.34 million tons per year, of which about 203000 tons are currently incinerated at Lithuanian CPP [3–5]. During the waste incineration process (to produce heat or energy), it generated about 11% of BA. After extracting metals, the BA is taken to the landfill and used for dumping. Although, there is a real opportunity to use generated BA in the construction industry. In some European countries such as France, Germany, and the Netherlands, BA is used to construct roads production of clay bricks and tiles [6–8].

Waste Directive 2008/98/EC provides the prevention of waste and the use of waste as a resource. Attempts should be made to recycle, reuse and dispose of waste [9]. The bottom ash is a mixture of slag, metals and other non-incineration materials. Its composition strictly depends on the composition of the waste incinerated [10].

Incineration of waste at a CPP takes in a boiler at 920–990 °C [4]. The efficiency and type of boiler affect the combustion quality. The organic part of the ash mainly consists of unincinerated cellulose and lignin obtained from plant materials contained in municipal solid waste (MSW).

Sintering is a thermal process of converting fine loose particles into a solid, coherent mass by heat and/or pressure without fully melting the particles [11]. This method is used in industry, especially in producing fired ceramic products and composite materials. This type of heat treatment of materials has advantages for industrial waste. During the sintering process, the inorganic part of the ash reacts with the minerals contained in the clays, and, as a result, new safety ceramic products are formed [12].

The solution to the problem associated with the accumulation of BA, an excellent solution is to use it as a substitute component in ceramic production. In works [13–16], it is reported that the ash obtained after incineration of waste can be used to produce silicate bricks, ceramic tiles, glass and glass ceramics.

In this work, the BA characteristics were studied, and mixtures of clay were prepared with various percentages of BA (10–40%) to investigate the possibility of reusing BA in ceramic products. The physical and mechanical properties of clay bricks have been studied; quantitative phase analysis of clay bricks fired at 900 °C and 1000 °C and determined the characteristics of the porous structure of materials, particularly the average pore size and pore size distribution had been completed. FTIR spectroscopy has determined the composition and structure of clay, bottom ash and clay bodies samples fired at a temperature of 900 and 1000 °C to study the interactions of clay minerals with inorganic or organic compounds.

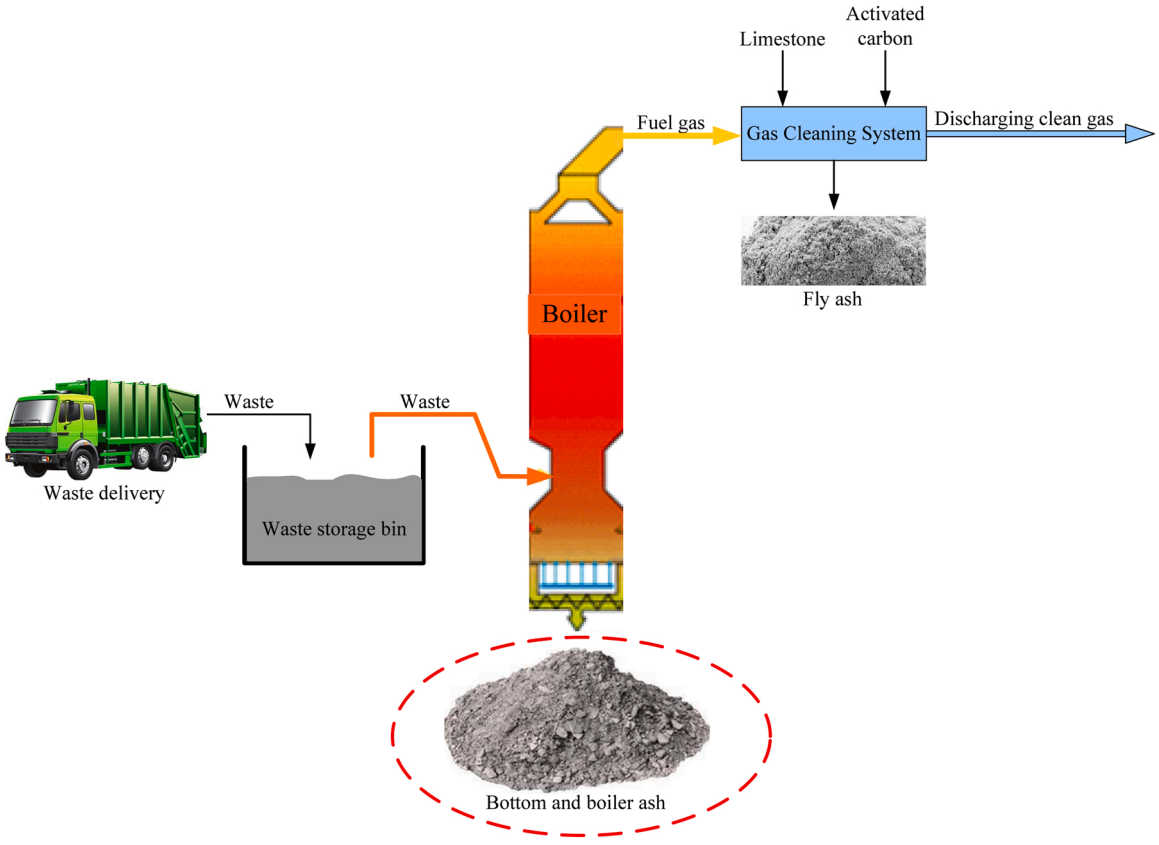

Fig. 1. The schematic process generation of bottom ash.

2. Materials and methods

2.1. Preparation of the test samples

The BA was obtained by incinerating refuse-derived fuel (RDF) at the cogeneration power plant. The waste incineration process occurs at a temperature of 900–950 °C. As a result of the waste incineration process at CPP, electricity is produced at 30%, heat is 60%, and by-products are generated at 10%. The schematic process generation of BA is presented in Fig. 1.

Currently, valuable metals are extracted from this by-product (BA), and the rest is sent to the landfill and used for dumping. After incineration, the generating BA can be disposed of as a replacement component in building materials. The BA samples were obtained from the Kaunas CPP (Lithuania). After four months of BA ageing in the atmosphere, the material samples for investigation had taken.

The clay used to form the samples was mined in the largest Andreevsky deposit in Ukraine, located near the city of Druzhkovka, Donetsk region, Ukraine. Clay Technik-3 has a high dry or fired mechanical strength, white colour after firing, low organic matter content, low water absorption, low drying sensitivity, wide sintering interval and stable quality. The clay humidity is 7%, and organic matter content has a low value of up to 5% [17]. The clay and BA were used in this experimental study. The materials (Fig. 2) have been dried at 105 ± 5 °C, crushed and sieved through a 0.63 mm sieve.

The samples were prepared from the clay and BA, previously dried to constant humidity. The components were mixed under dry conditions; water was added to the mixture (8%). The index of plasticity of the moulding mass practically did not change with the addition of ash residue (Table 1). The plasticity of the clay was determined by the standard Vasiliev cone method. The samples were pressed in steel molds at a pressure of 120 kg/cm^2. After pressed there were obtained small cube bricks 20 × 20 × 20 mm size. The formed samples were dried in an oven (SNOL 58/350) until a constant weight was established (≈24 h).

The dried samples were fired at 900 and 1000 °C for one-hour in the electric muffle furnace (SNOL 8.2/1100). The heating rate that was used during firing samples presented in Fig. 3.

In the temperature range of 25–200 °C, the samples were slowly heated to 75 °C/hour. In this interval, interlayer and partially adsorbed water were removed. In the temperature range of 200–400 °C, the temperature rise rate was 100 °C/hour. Upon reaching 400 °C, an exposure of 15 min was made to remove the evolved gases and equalize the temperature in the kiln space. The temperature range of 400–600 °C is characterized by the hydration of clay minerals and the release of chemically bound water included in the crystal lattice. The rate of temperature rise was 100 °C/hour, and upon reaching 600 °C, an exposure of 20 min was made. Upon reaching 600–800 °C, the rate of temperature rise was 130 °C/hour. In the temperature range of 800–1000 °C, the sintering process began. During sintering, diffusion transfer of matter occurs through chemical interaction of components and new minerals' formation. The rate of temperature rise in such firing was 75 °C/hour. The fired products were cooled down to the ambient temperature in the kiln.

2.2. Test instrument

The BA and clay's morphology and elemental analysis was investigated by applying scanning electron microscopy equipped with an energy dispersive spectroscopy detector (SEM-EDS). The analysed samples were passed through sieves and then subjected to drying at 40 °C. For SEM images the specimens (except powder) were cut into smaller sizes of about 5 × 5 × 5 mm and coated using gold (Au) prior to the morphological observation. SEM, observation of samples was performed on ZEISS EVO MA10 microscope at an accelerating voltage of 20 kV. Bruker AXSX Flash 6/10 Detector can display all the elements present in the specimen at overall accuracy of about 1% and detection sensitivity down to 0.1% by weight.

The properties of bottom ash and clay were determined by the following standards:

- Loss on ignition: LST EN 15935:2012;
- Bulk density: LST EN 13041:2012;

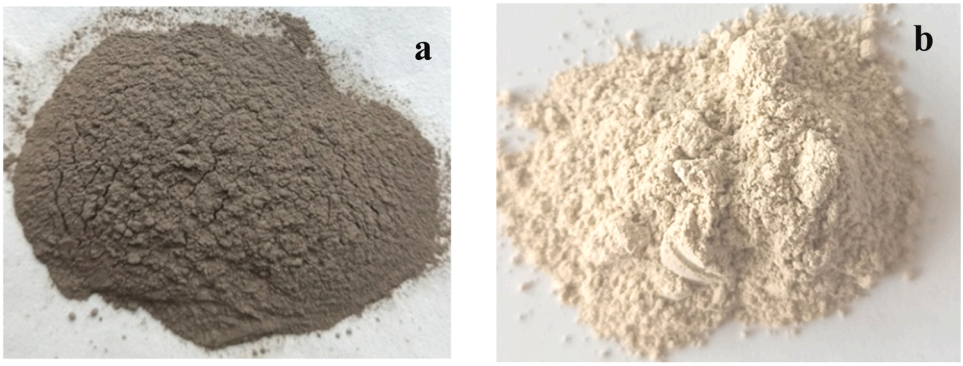

Fig. 2. Bottom ash after incineration of MSW (a) and clay (b).

Table 1
Composition of moulding compounds.

Raw materials	Composition of moulding compounds, %wt				
	BA0	BA10	BA20	BA30	BA40
Clay	100	90	80	70	60
Bottom ash	0	10	20	30	40
Moisture content (optimum)	8	8	8	8	8
Atterberg limits:					
Liquid limit	38	39	40	41	42
Plastic limit	21	23	25	27	30
Plasticity index	17	16	15	14	12

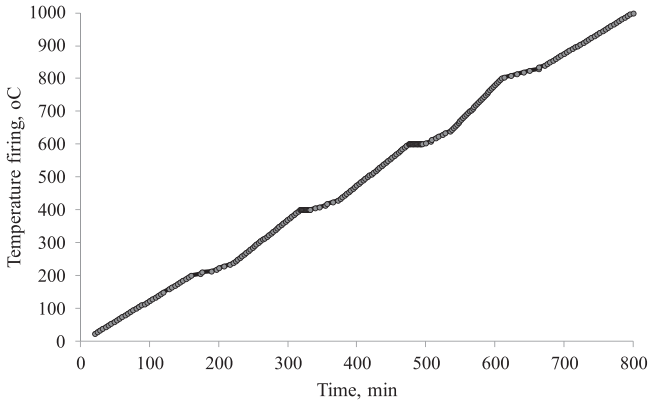

Fig. 3. The heating rate in the kiln.

– Dry solid content: LST EN 15934:2012, method A;
– pH: LST EN 15933:2012

The element analysis of BA and clay to determine metals was performed using an ICP-OES, Optima 8000 (Perkin Elmer). The samples (0.4–0.5 g) were mineralized with 8 ml of concentrated nitric acid, 1 ml of hydrofluoric acid and 3 ml of hydrogen peroxide at 800 W,6 MPa, pRate: 50 kPa·s^{-1} (Multiwalve 3000). After the mineralization, the solution was poured into 50 ml flasks and diluted to 50 ml using deionised water. For the data acquisition of the samples, a quantitative analysis mode was used. The scanning of every single sample during element analysis was repeated three times to gather reasonably good results. Analysis was made in four replicates of each sample.

Differential thermal analysis was done using Simultaneous Thermogravimetry and Differential Scanning Calorimetry (TG-DSC) – High-Pressure ability (STA PT 1600 (TG-DSC).

Fourier Transform Infrared Spectroscopy (FTIR) clay, BA, and clay bodies samples fired at 900 and 1000 °C were carried out. Infrared spectroscopy was conducted through the Fourier transform of adsorbent samples before and after adsorption. Samples were analysed in ALPHA Platinum ATR-FTIR spectrophotometer in the 4000–400 cm^{-1}region.

The physical and mechanical properties of the fired clay bricks were determined by the following standards:

– Density: LST EN 772–13:2003;
– Water sorption: LST EN 772–21:2011;
– The compressive strength: LST EN 772–1:20114;
– Freeze and thaw resistance: LST 1985:2006;
– The thermal conductivity. Hot-wire methods: LST EN 993–14:2001/P: 2006.

The drying and firing shrinkage of clay bodies were calculated according to the Eqs. 1 and 2.

$$S_{drying} = [(S_0 - S_1)/S_0] \cdot 100\% \quad (1)$$

$$S_{firing} = [(S_0 - S_2)/S_0] \cdot 100\% \quad (2)$$

where S_0 — distance between two reference marks in a wet sample, mm; S_1 distance between two reference marks in a dried sample at 105 °C, mm; S_2 — distance between two reference marks in a fired specimen at 900 and 1000 °C, mm.

X-ray diffraction analysis (XRD) of BA, clay and clay bricks were carried out on BRUKER D8 ADVANCE diffractometer with CuKα radiation at 40 kV in 2Θ (3°÷70°) interval at scanning step 0.02°. The obtained X-ray patterns were deciphered using the Diffract Eva program. Rietveld quantitative phase analysis was adopted for the quantitative phase analysis of clay bricks. The measurement

uncertainty was about ± 1 wt%.

Pore size distribution was obtained by the nitrogen adsorption method using the Quenched solid density functional theory (QSDFT), which considers the roughness and heterogeneity of the pore wall surfaces. Some researchers [18,19] use the BJH (Barret, Joyner and Halenda) and the method Mercury Intrusion Porosimetry (MIP) to describe the pore-size distribution, assuming cylindrical pore geometry in the clay materials. According to [20], clays are typical natural nanomaterials with a high sorption capacity. Colloidal forms of sulphides, silica and other compounds take an active part in the sorption of metals. It was decided to use the QSDFT method to consider the pore walls' heterogeneity and reliably characterize mesoporous in the range from 2 to 35 nm. The QSDFT method [21] makes it possible to analyse a broader range of pores.

Two-sided confidence levels with 95% mean values (water sorption, total open porosity, density, linear shrinkage and compressive strength) were calculated, assuming that water sorption, porosity, density, shrinkage and compressive strength usually are fixed random values. The Student's t-distribution was used to calculate the confidence levels.$(M - td,\ (1-\alpha/2)\cdot S/n^{0.5}) \le \mu \le (M + td,\ (1-\alpha/2)\cdot S/n^{0.5})$ of the means measurements, where M is estimates of the mean, S are standard deviation of random variables; n = 6 is the sample size, $td,\ (1-\alpha/2) \approx 2.6$ is $(1-\alpha/2) = 0.97$ quantile of the Student's t-distribution, $\alpha = 0.05$ is a level of significance and degree of freedom d= 5.

3. Results and discussion

The experimental tests by SEM-EDS analysis of clay showed that SiO_2 content is 66.65%, Al_2O_3 +TiO_2 content is 27.64%, CaO content is 0.2%, and the Fe_2O_3 content is 1.51%.

The experimental tests for analyzing the chemical composition of BA showed that SiO_2 content in the BA is 35.53%, Al_2O_3 +TiO_2 content is 10.3%, and the Fe_2O_3 content is 8.83%. The particle size distribution BA and clay showed in Table 2.

The analysis microstructure of clay and BA is presented in Fig. 4. Clay particles had a shape of 1.5–10 μm and were distributed almost evenly. Clay minerals belong to the layered and stratified-strip silicates of aluminium, iron and magnesium. Clay particles are predominantly lamellar, but there are also elongated plates and stripes and tubular and fibrous particles. The morphology and size of particles are associated with the features of their crystal structure. The BA particles were dark grey and had a lamellar and crystal shape. The bottom ash size range from 1 μm to 10 μm.

The main source of clays are feldspars, the destruction of which, under the influence of atmospheric agents, forms silicates of the group of clay minerals. The composition of feldspars is determined by the ratio of the components of the ternary system $NaAlSi_3O_8$-$KAlSi_3O_8$-$CaAl_2Si_2O_8$. There are two series of minerals: alkali-isomorphic mixtures $KAlSi_3O_8$ and $NaAlSi_3O_8$; plagioclase-isomorphic mixtures $NaAlSi_3O_8$ and $CaAl_2Si_2O_8$. At high temperatures, there are continuous series of solid solutions within each series (Fig. 5).

Among plagioclases, there are distinguished ($CaAl_2Si_2O_8$ content in mole %) is indicated in brackets: albite (0−10), oligoclase (10−30), andesine (30−50), labradorite (50−70), bytownite (70−90) and anorthite (90−100). Alkaline feldspars are distinguished ($NaAlSi_3O_8$ content in mole %) is indicated in parentheses: sanidine (0−63), orthoclase (0), microcline (0), which are polymorphic modifications $KAlSi_3O_8$ and anorthoclase (63−90). At low temperatures, solid solutions of alkali feldspars decompose into sodium and potassium phases, and in the $NaAlSi_3O_8$-$CaAl_2Si_2O_8$ system, plagioclases of a complex domain structure are obtained with a $NaAlSi_3O_8$ content of 2–16, 48–58 and 70–90 mol%.

The prevailing minerals in the clay detected by XRD analysis (Fig. 6) are quartz (28.99%), muscovite, titanium oxide (1.45%), kaolinite (3.86%), illite (9.09%), microcline (30.02%) and albite (3.62%) and correspond to the data [23].

The research found that BA content has an inorganic component, and the humidity was 6%. The incineration process of waste transforms organic materials in CO_2 and H_2O but yields inorganic residues from ferrous non-ferrous metals to silicates. X-ray diffraction analysis (Fig. 7) and FTIR spectra (Fig. 9) of BA evidence the presence of inorganic components.

Table 3 presents the results of element quantitative analysis and other properties bottom ash and clay.

According to the analysis results, the chemical elements found in clay and BA does not pose a severe threat to the environment since they do not contain heavy metals in their composition. Thus, according to data [24] and obtained by us, the bottom ash is classified as non-hazardous waste and can be used as an additive in ceramic production.

Fig. 8 shows DTA and TGA curves for clay and bottom ash. The DTA curve for clay has three endothermic peaks. The first one peak at 95 °C, the second one at 505 °C and the third one at 569 °C. The first peak TGA curve shows a weight loss of 1.45% at 120 °C, a 1.38% weight loss between 120 and 405 °C. The second and third peak TGA curve shows a weight loss of 3.12% between 410 and 592 °C. The total mass loss consisted of 7.84%. The endothermic peak and weight loss in the temperature range of 100–200 °C are due to the heating of products and the removal of interlayer and partially adsorbed water. In the temperature range of 200–300 °C, the

Table 2
Chemical and granulometric composition of the clay and BA.

Raw materials	Chemical composition, %											
Clay	SiO_2	Al_2O_3	K_2O	TiO_2	Fe_2O_3	MgO	Na_2O	CaO	SO_3	P_2O_5	other	**Total**
	66.65	25.72	2.8	1.92	1.51	0.66	0.53	0.2	—	—	0.21	**100**
Bottom ash	35.53	8.68	0.67	1.62	8.83	3.71	5.48	30.46	2.62	1.26	1.08	**100**
	Granulometric composition, %											
	> 0.5 mm			0.5–0.063 mm			0.063–0.01 mm			> 0.01 mm		
Clay	0.2			1.8			22.4			75.6		
Bottom ash	0.18			2.5			75.8			21.5		

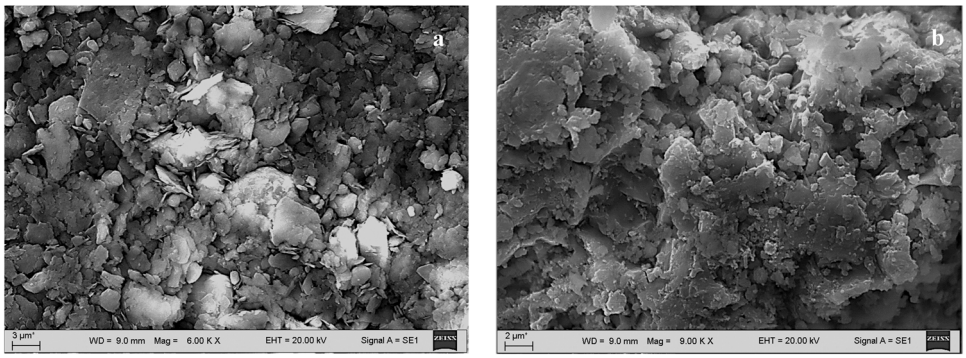

Fig. 4. Microstructure clay (a) and BA (b).

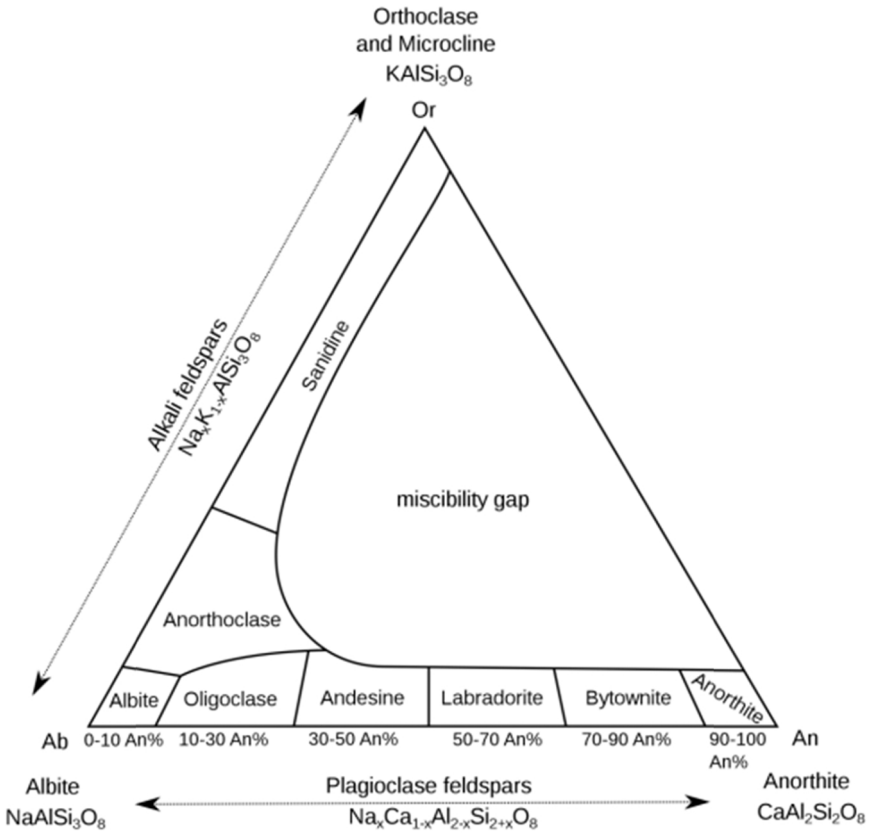

Fig. 5. Ternary phase diagram of the feldspars [22].

removal of bound water is completed, and some of the organic substances are burned. Distinct endothermic peaks and weight loss in the temperature range of 505 and 569 °C are due to the dehydration of clay minerals and the release of chemically bound water included in their crystal lattice [25].

The situation is similar for DTA and TGA curves for bottom ash. The DTA curve for bottom ash has two endothermic peaks at 100 °C and 781 °C. The first peak TGA curve shows a weight loss of 1.55% at 100 °C, a 3.33% loss between 110 and 620 °C. The second peak TGA curve shows a weight loss of 3.47% between 669 and 750 °C and a 15% loss between 620 °C and 760 °C. The total mass loss was 9.39%. The endothermic peak and weight loss in the temperature range of 100–200 °C are due to the removal of residual moisture. In the temperature range of 300–500 °C, there was a burnout of organic inclusions and the removal of "crystallization" water. Distinct endothermic peak and weight loss at 790 °C are due to the decomposition of carbonates, accompanied by the release of carbon dioxide [26]. With the release of gaseous components released during the decomposition of carbonates, cracks can appear on the surface of the matrix and weaken the interaction of particles.

Fig. 9 shows FTIR spectra obtained for clay and BA. Bands of clay at about 3700 and 3400 cm^{-1} are characteristic —OH stretching

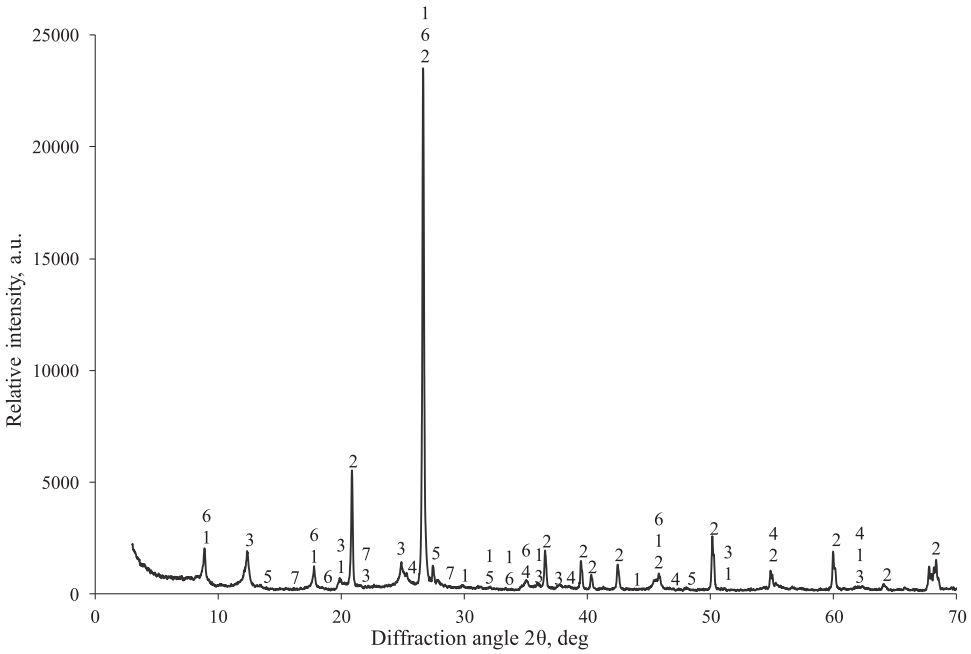

Fig. 6. The clay XRD analysis: 1 – muscovite, 2 – quartz, 3 – kaolinite, 4 – titanium oxide, 5 – microcline, 6 – illite, 7 – albite.

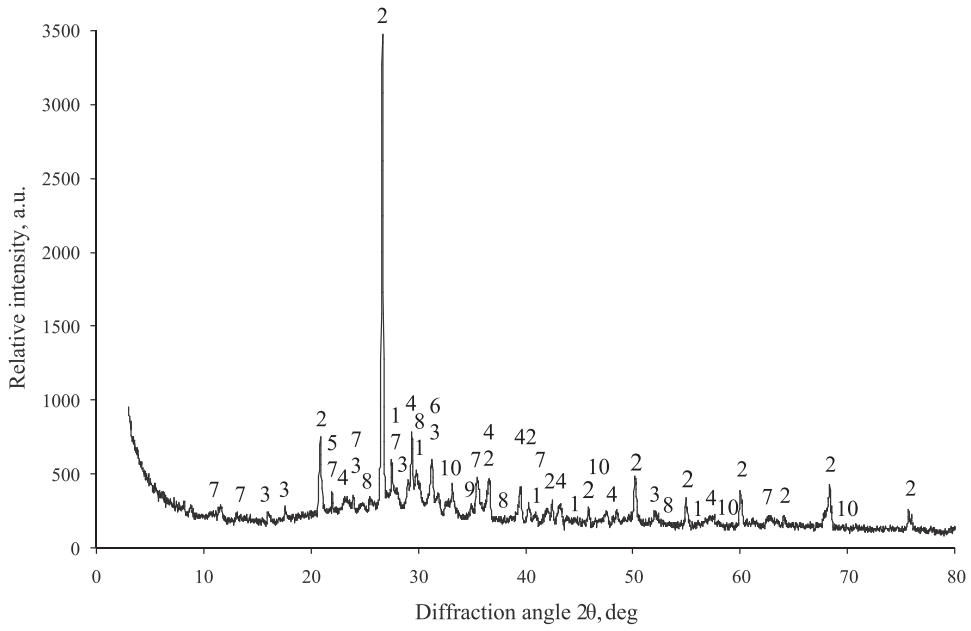

Fig. 7. The bottom ash XRD analysis: 1 – diopside; 2 – quartz; 3 – akermanite; 4 – calcite; 5 – cristobalite; 6 – gehlenite; 7 – albite; 8 – wollastonite; 9 – iron oxide; 10 – perovskite.

regions; these two bands are assigned to the —OH stretching vibration of the structural hydroxyl groups in the clay and the water molecules present in the interlayer, respectively [27] group vibration elongation. The small absorption band for clay and BA at 1630 cm^{-1} are due to adsorbed water presence in clay [25].

The characteristic strong peaks at 876 cm^{-1} and 1430 cm^{-1} correspond to the C–O bonding of $CaCO_3$, which corroborated the presence of $CaCO_3$ in bottom ash. The band attributed to Si-O occurs in the 1035 cm^{-1} region, while 920 cm^{-1} suggests Al-OH-Al [25] deformation vibration. Quartz peaks with different Si-O and Si-O-Al vibrations were detected close to 790 and 690 cm^{-1}, and bands close to 530 and 460 cm^{-1} indicate the typical elongation of the Si-O-Al bond [26].

After firing ceramic specimens at 900 and 1000 °C without adding BA and with adding it, defects such as swelling and cracking

Table 3
Element quantitative analysis and other properties bottom ash and clay.

Species	Results				
	Bottom ash	Standard deviation, %	Clay	Standard deviation, %	Unit of measurement
Silicium (Si)	181625.6	± 16.7	337729	± 15	mg/kg
Calcium (Ca)	168099.8	± 12.7	40.7	± 24.4	mg/kg
Ferrum (Fe)	51532.6	± 9.3	2960.6	± 14.8	mg/kg
Aluminшum (Al)	33396.4	± 4.9	17066.9	± 12.5	mg/kg
Natrium (Na)	26178.5	± 6.6	1774.2	± 14.6	mg/kg
Magnesium (Mg)	15250.4	± 22.9	333.6	± 18.4	mg/kg
Kalium (K)	11128.2	± 9.4	9903.9	± 6.4	mg/kg
Titanium (Ti)	6428.1	± 16.2	7447.3	± 11.8	mg/kg
Sulfur (S)	4487.2	± 6.9	< 1.8		mg/kg
Zincum (Zn)	3762.8	± 26.1	2.0	± 11.3	mg/kg
Cuprum (Cu)	3498.7	± 19.1	28.7	± 12.3	mg/kg
Phosphorus (P)	2400.1	± 14.6	< 3.5		mg/kg
Chromium (Cr)	743.6	± 10	74.6	± 14.4	mg/kg
Manganum (Mn)	668.8	± 11.9	38.4	± 16.5	mg/kg
Dry solid content	977	± 13	946	± 12	g/kg
Bulk density	1101	± 20	1400	± 22	kg/m^3
pH	8.5	± 0.2	7.5	± 0.5	pH value
Loss on ignition	7.75	± 0.5	5.4	±0.5	%

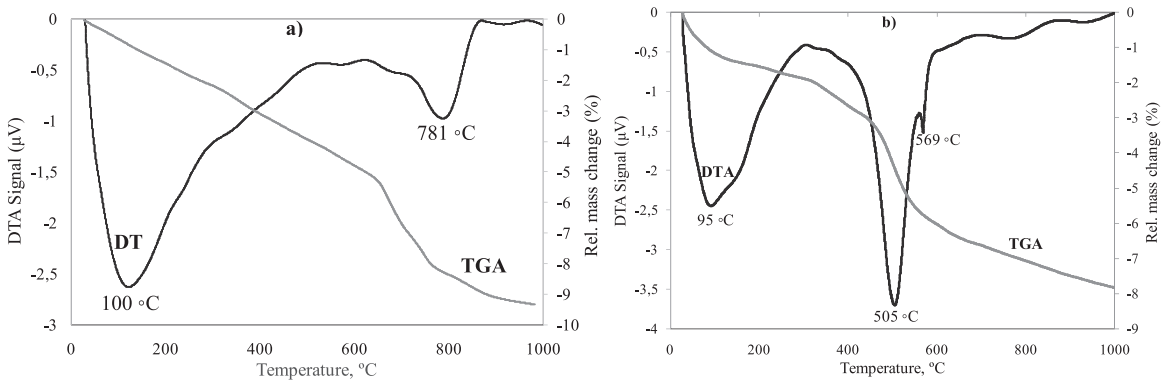

Fig. 8. DTA and TGA curves of bottom ash (a) and clay (b).

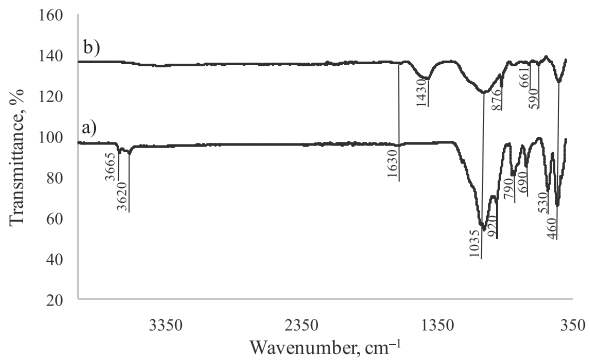

Fig. 9. FTIR spectra for clay (a) and bottom ash (b).

were not observed. A colour change was observed in the finished fired samples. Colour saturation increased with increasing BA addition. In some samples with the BA40 and firing at 1000 °C, small dark-grey coring appeared in the form of a dot. It is known that during firing, at a temperature of 800–1000 °C, calcium $CaCO_3$ and magnesium carbonates $MgCO_3$ actively interact with decomposition products of clay minerals — amorphous silica SiO_2 and alumina Al_2O_3. These reactions proceed with the release of carbon dioxide CO_2. Some colouring oxides — manganese MnO_2, copper CuO, iron Fe_2O_3, decompose during firing, releasing oxygen O_2. Most likely, such chemical transformations could provoke the appearance of such a defect. In the ceramic mixture, when heated, chemical

and physicochemical processes proceed sequentially, leading to a complete and irreversible change in its structure: removal of chemically bound water; decomposition of dehydrated clay into oxides Al_2O_3 and SiO_2; formation of new water-resistant and refractory minerals; formation of a certain amount of melt from low-melting clay.

The formation of a durable product occurs due to the adhesion of solid particles of clay and BA by the resulting melt. In this case, due to the forces of surface tension of this melt, a decrease in the volume of the material occurs, called fire shrinkage. Shrinkage during drying of clay masses without adding ash residue reached 5.15%; the shrinkage during firing at 900 °C was 6.25%, and at 1000 °C, the shrinkage reached 7.14%. The shrinkage of the ceramic products during firing depends on the amount of BA added. Depending on the moulding composition, the shrinkage during firing at 900 °C varies from 5.93% to 5.03% and from 6.69% to 5.55% at 1000 °C (Fig. 10).

Shrinkage occurs due to a decrease in the thickness of the water shells around the clay particles, forming a framework of ash residue minerals and the convergence of particles under the action of capillary pressure forces. This frame prevents the clay particles from coming together during drying. Fire shrinkage during firing occurs as a result of the general effect of all physicochemical processes occurring in the ceramic mass during firing — dehydration of minerals, material transfer due to diffusion, recrystallization and the formation of new minerals, as well as due to the convergence of particles under the action of surface tension forces of liquid phases during sintering. For the samples under consideration, fire shrinkage is relatively small. This occurs due to the formation of new minerals or the recrystallization of the former.

The density of the fired clay samples without the addition of BA varied with the firing temperature. The density of the samples during firing at 900 °C was 1.99 g/cm^3 and at 1000 °C — 2 g/cm^3, respectively. With the addition of 10% BA, the density of the samples decreased and amounted to 1.93 and 1.99 g/cm^3 at the same temperatures. An increase in the additive content in the ceramic mass led to a decrease in the density of the samples. Therefore, with the addition of 40% BA, the density was 1.85 and 1.88 g/cm^3 at temperatures of 900 °C and 1000 °C, respectively (Table 4). The compressive strength of clay samples depends on BA content and the firing temperature. With an increase in the BA content decrease in the density of the samples and the compressive strength.

The clay samples with a BA30 and fired at 1000 °C had a sufficiently high compressive strength of 14.5 MPa and can be used to construct buildings and structures. While ceramic samples with the same percentage of BA, fired at a temperature of 900 °C, had a compressive strength of 10.6 MPa. The compressive strength decreases due to the combustion of adhesive additives, dehydration of clay minerals, and chemical transformations inside the sintered ceramic mass. The main chemical transformation is calcite decarburization. According to [28,29], the compressive strength of a brick prepared under laboratory conditions for testing should not be lower than 20 MPa. The European Union standard does not specify minimum values for compressive strength. Accordingly, each manufacturer must declare compressive strength clay bricks, and according to this data, designers must consider these values when designing structures. However, it is known that the compressive strength of clay bricks must be at least 10 MPa.

Water sorption and open porosity depend on the size, number and distribution of pores in the clay brick and are important for ceramic products. There was a significant difference in water sorption and open porosity values for clay bricks fired at 900 and 1000 °C. The lowest values for water sorption and open porosity had samples fired at 1000 °C without adding BA. These clay brick samples had a water sorption value of 11.4% and an open porosity of 24.1%. With 10% BA, water sorption and open porosity increased to 11.7% and 25%, respectively. With the subsequent addition of 20%, 30% and 40% BA, clay brick samples' water sorption and open porosity increased. Clay samples fired at 900 °C had water absorption and open porosity values higher than samples fired at 1000 °C.

Requirements for water absorption in clay brick samples are not specified by the European Standard LST EN 771–1:2011 +A1:2015. Based on this, manufacturers must indicate the water absorption values for their products in accordance with the standard LST EN 772–21:2011. Permissible water absorption for clay bricks must consist of 12–20%. If the water absorption value is below 12%, it may lead to improper bonding between mortar and bricks.

The physical and mechanical properties presented above are interconnected with the microstructure formed in the samples. It is known that the microstructure, properties and clay bricks depend on the pores, their distribution and interaction with water. The firing process at higher temperatures increases the crystallization process, resulting in intensive sintering of clay minerals, an increase in the volume of the liquid phase, a glass phase increase, a decrease in porosity and closing of the open pores of the samples. Phase and

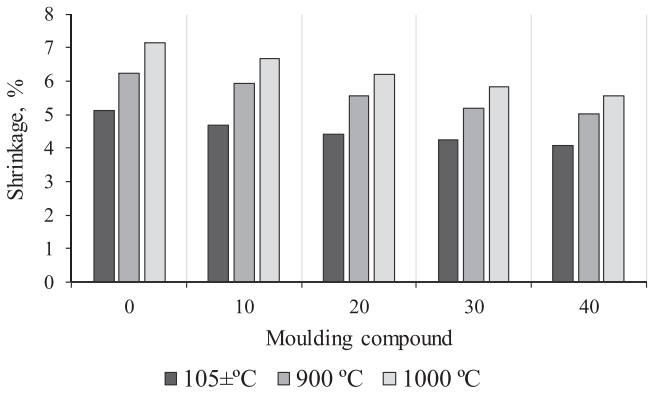

Fig. 10. Linear shrinkage of clay brick specimens.

Table 4
Properties of clay bricks samples.

Properties	Ceramic samples Firing temperature $\frac{900^oC}{1000^oC}$				
	BA0	BA10	BA20	BA30	BA40
Water sorption, %	$\frac{13.9 \pm 1.1}{11.4 \pm 1.4}$	$\frac{14 \pm 1.5}{11.7 \pm 1.7}$	$\frac{14.2 \pm 1.3}{12.1 \pm 1.5}$	$\frac{14.7 \pm 1.8}{13.1 \pm 2.0}$	$\frac{16.3 \pm 2.0}{15 \pm 2.4}$
Total open porosity, %	$\frac{24.4 \pm 1.8}{24.1 \pm 2.1}$	$\frac{27.3 \pm 2.2}{25 \pm 1.6}$	$\frac{28.4 \pm 1.9}{25.7 \pm 2.0}$	$\frac{28.9 \pm 2.2}{26 \pm 1.9}$	.
Density, g/cm^3	$\frac{1.99 \pm 0.003}{2 \pm 0.002}$	$\frac{1.93 \pm 0.002}{1.99 \pm 0.002}$	$\frac{1.92 \pm 0.002}{1.97 \pm 0.004}$	$\frac{1.90 \pm 0.003}{1.92 \pm 0.002}$	$\frac{1.85 \pm 0.004}{1.88 \pm 0.003}$
Compressive strength, MPa	$\frac{21.2 \pm 0.9}{26.2 \pm 1.21}$	.	$\frac{12.7 \pm 1.2}{17 \pm 1.4}$	.	$\frac{6.3 \pm 1.5}{9.9 \pm 1.4}$
Thermal conductivity, W/m·K	1.1/1.02	0.75/0.69	0.61/0.57	0.56/0.53	0.53/0.49

structural changes in clay samples with the addition of BA lead to a decrease in density, compressive strength, an increase in water absorption and total open porosity [30]. Clay samples with high additive BA have a more significant number of open pores and capillaries formed due to high-temperature transformations of the minerals contained in BA and decarbonisation of calcium carbonate. The resulting pores affect the physical and mechanical properties of clay samples.

There is a little difference between the morphology and appearance of the surfaces of clay bricks BA0 and with BA10. The microstructure of samples is dense with a predominance of a small number of pores. The pores are small and relatively evenly distributed throughout the sample. The microstructure of clay brick sample BA20 has different: the surface is less uniform with a predominance of pores of various sizes. The pores develop due to the intensive removal of CO_2 during the firing and decomposition of calcium carbonate. The fact that the amount of carbon in the samples increases is evidenced by the SEM-EDS analysis of the samples. The thermo chemical transformations of clay minerals and BA occur, as evidenced by the data presented in Fig. 11. These data show that some elements decrease with the addition of ash residue, for example, oxygen, silicon, aluminium, potassium, and some increase.

The microstructure of samples BA30 is different: bigger pores of various shapes predominate, formed due to intensive removal of crystal water and removal of gas components (CO_2, O_2) during the interaction of $CaCO_3$ and $MgCO_3$ the decomposition of colourful oxides (Fe_2O_3). An increase in the content of calcium, magnesium and iron is evidenced by the analysis data.

Frost resistance is an essential step of study that must be carried out without fail [31]. Formed and fired samples of ceramic bricks were subjected to freeze and thaw resistance testing and visual evaluation. The reference sample and samples with BA10–30, fired at 900 °C, completed 25 freezing and defrosting cycles (the cycle consists of one freezing phase at —18 °C and one thawing phase at +18 °C). The samples BA40 and fired at 900 °C completed 23 freezing and defrosting cycles. All samples (control and with the BA) fired at 1000 °C completed 25 freezing and defrosting cycles. Based on LST EN 771–1:2011 +A1:2015, these products can be operated in passive and moderate aggressive environments.

The thermal conductivity analysis was performed on clay brick patterns mixed with BA of 0, 10, 20%, 30% and 40% by weight and fired at 900 and 1000 °C. The relationship between thermal conductivity and porosity of clay bricks with the addition of BA can see in Table 4. An increase in the percentage of BA likely causes an increase in the porosity of the samples. The results show that a higher percentage of BA addition causes low thermal conductivity in the samples. This is a result of the increase in air volume produced by the interaction of clay minerals with BA, which leads to the formation of pores within the samples, making them poor heat conductors and, as a result, good insulators. The results show that thermal conductivity decreases with decreasing density and increasing porosity of fired clay bricks. As a result, the thermal conductivity values directly depend on the porosity. The thermal conductivity values for samples without the addition of BA and with the addition of it were in the range of 0.49–1.1 W/m·K. Based on the ASTM D 78896 standard, it can be argued that the addition of bottom ash during the production of bricks does not impair the technical properties of the fired samples.

The infrared spectra of the clay bodies with BA from 0% to 40% and fired at 900 and 1000 °C are presented in Fig. 12. The clay samples fired at 900 °C characterized the following bands. The characteristics band of 1150 cm^{-1} correspond to the stretching vibration modes of SO_4 tetrahedron.

The other bands at 1033, 1037 cm^{-1} are those of Si—O bonds. The presence of a doublet at 792 and 778 cm^{-1} (for 1000 °C) and 798 and 774 cm^{-1} (for 900 °C) are attributed to the quartz vibrations. Quartz peaks with different Si-O and Si-O-Al(Mg) vibrations were detected close to 690, and 680 cm^{-1}, bands close to 560 and 562 cm^{-1} indicate the typical elongation of the Si-O-Mg and bands close to 450 and 453 cm^{-1} indicate the Si-O-Al bond [32]. This result is in accordance with that of XRD patterns.

Powder diffraction is one of the most widely used analytical techniques for characterizing solid-state materials. The XRD-Rietveld refinement method can be used for phase identification, quantitative analysis, cell parameter determination, or complete crystal structure analysis. Fig. 13 (a) presented the XRD pattern (2θ=5–70°) of control samples of clay bricks with BA10–40 and fired at 900 and 1000 °C. Fig. 13 (b) shows the XRD analysis by Rietveld refinement of clay bricks with BA40 (using the Topas program).

Table 5 shows the data of the XRD Analysis by Rietveld refinement of reference samples and samples with the addition of bottom ash and fired at 900 and 1000 °C. Quartz is the main mineral in fired samples [33]. During the firing of ceramic specimens, the percentage of quartz changes. At the firing of 900 °C, the amount of quartz changed from 76.48% to 60.22% and from 86.71% to 58.97% at 1000 °C, respectively. The clay mineral illite [34–36] is present only in the reference samples and is 3.12% at firing 900 °C and 0.94% at 1000 °C. The presence of muscovite 2M1 [32] is typical in all samples but with different content (from 8.06% to 9.21% at

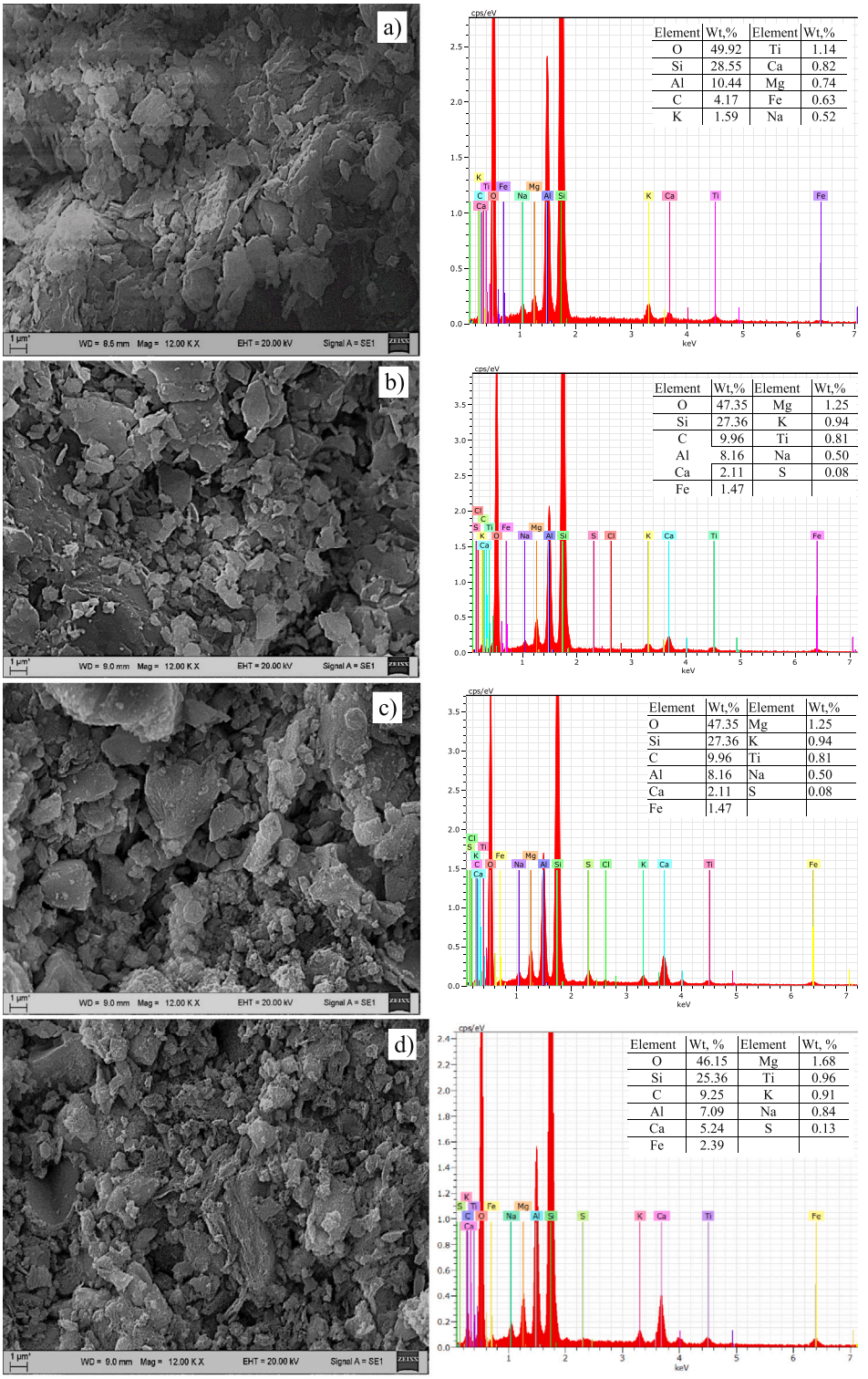

Fig. 11. SEM-EDS analysis of clay brick samples fired at a temperature of 1000 °C: sample BA0 (a), sample BA10 (b), sample BA20 (c), sample BA30 (d).

firing 900 °C and from 1.85% to 3.2% at 1000 °C).

The presence of anorthoclase [37] is characteristic of all samples and increased with the amount of BA and temperature firing (from 1.93% to 4.53% at 900 °C and from 1.32% to 3.62% at 1000 °C). An increase in the percentage of anorthoclase indicates an

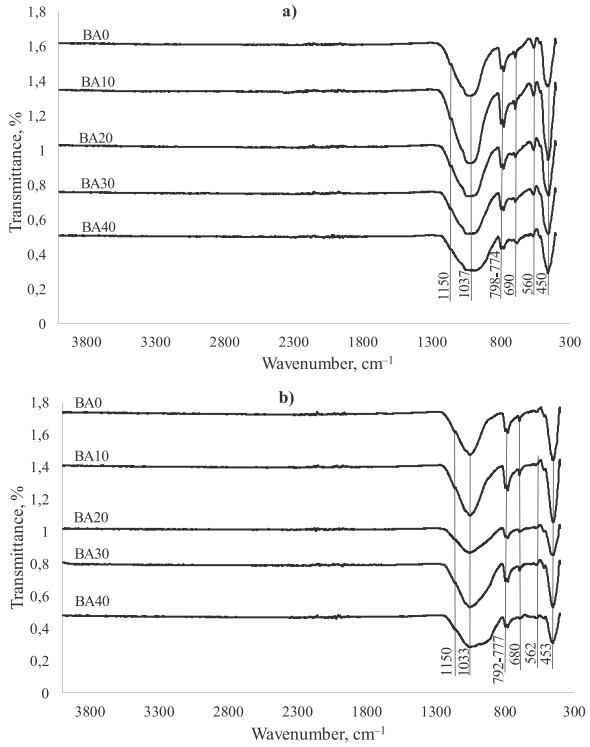

Fig. 12. FTIR spectra for clay bodies samples with different amounts of BA and fired at 900 °C (a) and 1000 °C (b).

improvement in the strength characteristics of clay samples. Microcline is an important raw material for the ceramic industry [36]. The microcline content in fired clay samples increases in proportion to the amount of BA and is from 1.26% to 6.83% at firing 900 °C and from 1.32% to 3.62% at 1000 °C, respectively. It should be noted the presence of cristobalite [38] in fired ceramic samples that contain the addition of BA. Therefore, in the ceramic samples fired at 900 °C, the presence of the.

cristobalite of 0.16–0.85%, at 1000 °C, the samples contending of 0.72–2.18%. According to [33,39,40], wollastonite is an industrial mineral comprised of calcium, silicon and oxygen. In the studied clay brick samples, the amount of wollastonite increases with the rising amount of BA and ranges from 0.85% to 3.1% at firing at 900 °C and from 1.29% to 4.13% at 1000 °C respectively. The samples contain wollastonite 2 M. Akermanite is a mineral of the melilite group [41]; it is also named a technogenic mineral. Akermanite is more durable than wollastonite. The content of akermanite increases with BA content and ranges from 0.24% to 2.06% at firing 900 °C and from 0.43% to 1.79% at 1000 °C. Gehlenite is contained in the fired clay brick samples [41]. It is a mineral of the silicate class, melilite group, forming a series with akermanite, with the same strength as akermanite. The gehlenite content is more than one per cent in samples with BA30 and BA40. In the rest of the samples, the gehlenite content is less than one per cent. In addition, less than one per cent is the mineral rutile [41]. It increases proportionally with the widening in the content of BA in the samples, regardless of the firing temperature.

As for hematite [42,43], this is a relatively common and durable mineral. The hematite content in the samples increases with an increase in the amount of BA from 0.15% to 2.04% at firing 900 °C and from 0.36% to 1.94% at firing 1000 °C. The presence of hematite results in a slight change in the colour of fired items. Labradorite [33,44] is feldspar of the plagioclase series (isomorphic mixture). In the samples under consideration, labradorite is formed in samples fired at 1000 °C beginning from BA20 and constitutes 1.5–5.45%.

According to [33,45], diopside is a mineral belonging to pyroxenes. With an increase in BA content in the samples, the diopside content also is enlarged from 0.67% to 3.23% at firing 900 °C and from 0.76% to 5.67% at 1000 °C. Diopside actively interacts with clay. An increase in diopside in the clay raw material intensifies the sintering process. It promotes the formation of an iron oxide melt, which acts as a flux and participates in the sintering of the material. According to [45], when diopside is presented into the clay mass, it improves the compressive strength and reduces the water absorption of the samples. In our case, this does not happen since, to fulfil such a condition, the content of the diopside must be more than 6%.

The structure of porous materials is usually formed in crystallization or subsequent treatment stages and consists of isolated or interconnected pores that may have similar or different shapes and sizes. Porous materials are characterized by pore sizes derived from gas sorption data [46]. According to IUPAC classification, pore sizes of clay brick samples fired at 900 °C and 1000 °C belong to the II type of isotherms (nonporous or macroporous). According to IUPAC [21], materials of fired clay bricks samples belong to the H3 hysteresis loop and are characterized by slit-shaped pores. The desorption curve of H3 hysteresis contains a slope associated with a force on the hysteresis loop due to the tensile strength effect [47]. Pore size distribution studies obtained from nitrogen adsorption

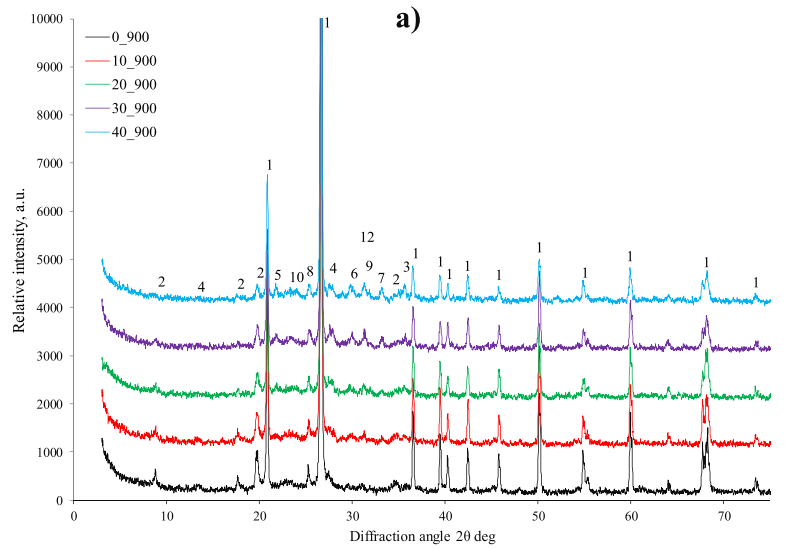

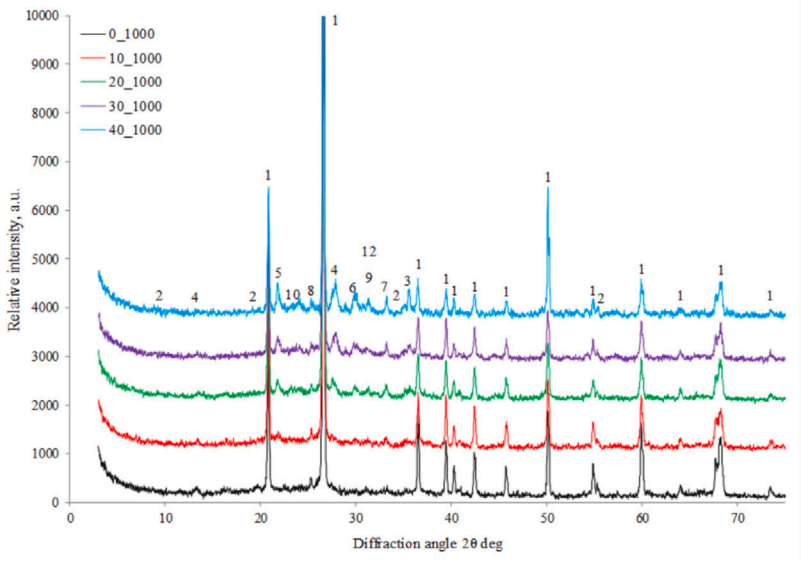

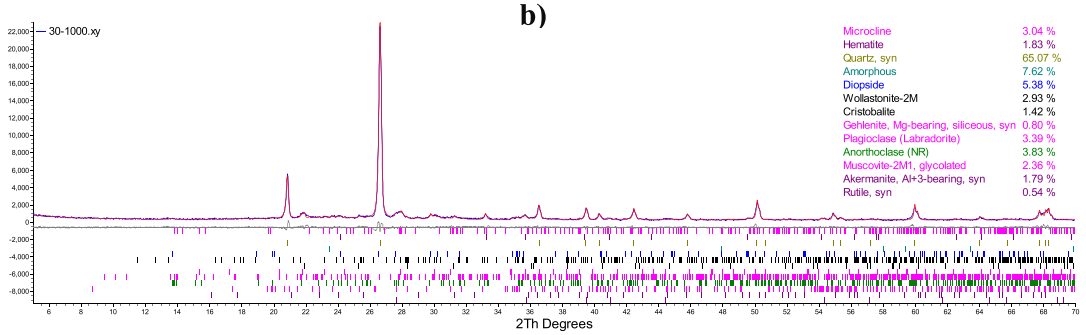

Fig. 13. XRD Analysis by Rietveld refinement of clay bricks: a — X-ray diffraction pattern of clay bricks fired by 900 and 1000 °C (1 – quartz, 2 – muscovite, 3 – hematite, 4 – microcline, 5 – cristobalite, 6 – diopside, 7 – wollastonite, 8 – rutile, 9 – gehlenite, 10 – akermanite, 11 – labradorite, 12 – anorthoclase); b — powder diffraction pattern for clay bricks with BA30 and fired at 1000 °C.

Table 5
Results of XRD analysis by Rietveld refinement.

Parameters	Temperature of firing, 900 °C										Temperature of firing, 1000 °C									
	Amount additive, wt%																			
	0		10		20		30		40		0		10		20		30		40	
Phases	w, %	d-spac., Å	w, %	d-spac., Å	w, %	d-spac., Å	w, %	d-spac., Å	w, %	d-spac., Å	w, %	d-spac., Å	w, %	d-spac., Å	w, %	d-spac., Å	w, %	d-spac., Å	w, %	d-spac., Å
Amorphous	6.68	3.85	7.81	3.8	8.56	3.73	7.37	3.7	7.45	3.64	5.56	3.89	6.25	3.9	6.33	3.81	7.62	3.79	8.31	3.59
Quartz	76.48	4.26	74.2	4.25	69.74	4.25	64.68	4.25	60.22	4.26	86.71	4.26	82.04	4.25	76.19	4.25	65.07	4.25	58.9	4.26
		3.57		3.34		3.34		3.34		3.34		3.34		3.34		3.34		3.34		3.34
		3.27		2.45		2.45		2.45		2.46		2.46		2.45		2.45		2.45		2.46
Muscovite 2 M1	8.06	10.04	8.32	10.07	8.88	10.05	9.21	10.11	8.34	10.02	2.53	10.05	3.13	10.03	3.2	10.01	2.36	10.01	1.85	9.93
		4.49		4.48		4.99		5.02		5.00		5.02		4.45		4.44		4.44		4.96
		3.35		3.5		4.48		4.47		3.31		3.52		3.48		3.48		3.51		3.49
Illite	3.12	4.46	—	—	—	—	—	—	—	—	0.94	20.04	—	—	—	—	—	—	—	—
		3.34										4.50								
		2.56										3.35								
Anorthoclase	1.93	4.08	2.81	4.05	3.09	4.07	4.53	4.08	4.16	4.08	0.92	4.02	1.28	4.02	1.79	4.06	3.83	4.08	4.38	4.09
		3.80		3.52		3.50		3.23		3.78		3.75		3.76		3.21		3.24		3.74
		3.25		3.24		3.24		3.47		3.24		2.53		3.09		2.99		3.0		3.23
Microcline	1.26	4.26	2.34	4.21	2.83	4.23	5.21	4.19	6.83	4.21	1.32	3.88	2	3.96	2.06	3.97	3.04	3.99	3.62	4.00
		3.57		3.51		3.51		3.51		3.49		3.50		3.5		3.51		3.44		3.20
		3.27		3.30		3.31		3.30		2.88		3.23		3.21		3.18		3.18		3.09
Cristobalite	—	—	0.16	4.1	0.36	4.04	0.64	4.06	0.85	4.06	—	—	0.72	4.06	1.21	4.05	1.42	4.05	2.18	4.04
				3.19		2.89		3.15		3.13				3.12		2.95		3.14		2.8
				2.85		3.12		2.84		2.90				2.92		2.52		2.48		2.52
Titanium oxide	0.44	3.24	0.5	3.29	0.75	3.24	0.44	3.24	0.7	3.18	0.31	3.25	0.31	3.23	0.19	3.24	0.54	3.22	0.7	3.23
		2.49		2.46		2.48		2.48		2.50		2.49		2.48		2.48		2.51		2.49
		2.19		2.17		2.29		2.18		2.18		2.29		2.28		2.28		2.19		2.19
Diopside	0.67	2.94	1.68	3.2	1.7	3.24	3.23	3.29	3.03	2.98	0.76	3.04	0.95	3.02	2.89	3.21	5.38	3.23	5.67	2.95
		3.04		2.98		2.99		3.22		2.55		2.54		2.93		2.97		2.99		2.98
		2.50		2.92		2.94		2.97		2.92		2.94		2.88		2.81		2.90		2.53
Wollastonite 2 M	—	—	0.85	3.86	1.36	3.84	1.43	3.82	3.1	4.04	—	—	1.29	3.87	1.68	3.33	2.93	3.5	4.13	3.82
				3.46		3.5		3.5		3.31				3.49		2.95		3.07		3.32
				3.0		2.96		2.96		2.97				2.97		2.78		2.97		2.97
Hematite	0.15	3.68	0.49	3.67	0.93	3.67	0.94	3.68	2.04	3.68	0.36	3.68	0.89	3.67	1.26	3.67	1.83	3.68	1.94	3.34
		2.70		2.69		2.69		2.69		2.70		2.70		2.69		2.69		2.69		2.68
		2.52		2.51		2.51		2.51		2.51		2.51		2.51		2.51		2.51		2.51
Gehlenite	0.18	2.76	0.2	3.05	0.56	3.04	0.75	3.04	1.22	2.82	0.17	2.88	0.51	3.05	0.9	3.23	0.8	3.19	1.7	2.86
		3.0		2.81		2.83		2.83		2.47		3.06		2.83		2.81		2.97		3.08
		2.98		3.0		3.83		3.67		3.02		2.76		2.42		2.72		2.57		3.71
Akermanite	0.24	2.79	0.63	3.7	1.28	3.07	1.75	3.06	2.06	2.85	0.43	2.87	0.59	2.85	0.84	3.69	1.79	3.06	1.1	2.84
		2.99		3.07		3.7		3.7		3.07		3.09		3.07		3.06		2.85		3.06
		2.37		2.85		2.85		2.85		3.71		3.73		3.71		2.85		3.7		3.7
Labradorite		—								—	—	—	—		1.5	4.09	3.39	4.08	5.45	4.08
																3.23		3.77		3.77
																2.5		3.21		3.21

experiments for samples fired at 900 °C and 1000 °C show a different trend when BA from 10% to 40% is included in the clay and at two firing temperatures. The BET-based method was performed using nitrogen as the adsorbate at a 77.35 K. The relationship between pore diameter, and the surface area was determined by the DFT method is shown in Fig. 14.

Fig. 14 shows that in the reference samples fired at 900 °C and samples with the addition of BA10, BA20 and fired at 1000 °C, micropores predominate in the remaining mesopores. Surface area and adsorption were obtained from the adsorption isotherm and calculated using a BET-based method. In addition, the total pore volume and average pore diameter were estimated using the DFT method, and all these data can be seen in Table 6.

The table data shows that the surface area of clay samples and the total pore volume decrease when BA is added to the base material for both firing temperatures. In addition, the average pore diameter of the samples without BA and with BA10, BA20 and fired at 900 °C had the same value (3.385 nm). However, with an increase in the amount of BA (30% and 40%) and a firing of 900 °C, the average pore diameter of the samples increased sharply and amounted to 26.12 and 33.242 nm, respectively.

Nevertheless, the average pore diameter of samples fired at 1000 °C has a different dependence. The pore size of samples without the addition of BA is 36 nm. Adding BA to the clay demonstrates a decrease in the pore diameter value at the same size. A positive correlation was found between the specific surface area and pore volume for samples fired at 900 °C. A similar trend is observed for samples fired at 1000 °C.

The data of nitrogen porosimetry can be compared with the studied microstructure of the samples. Samples fired at 900 °C demonstrate two groups of porosity, 3 nm and 4.5 nm. The pores of the first group correlated to the porosity of BA0, BA10 and BA20 samples, and the second group to the porosity with BA30 and BA40 samples. In all samples fired at 900 °C, the group of pores had a bimodal distribution, where pores of smaller diameter referred to slotted pores of clay material, and pores of larger diameter referred to slotted and cylindrical pores, which are formed as a result of thermo-chemical transformations of BA and clay minerals. The formation of cylindrical pores and an increase in the pore diameter in samples BA30 and BA40 fired at 900 °C is explained by the rise in the percentage of BA. This is explained characterized by compaction of the structure of ceramic materials as a result of contact sintering of the spherical vitreous substance of particles of amorphous clay aggregates and other components of the clay mixture, as well as by the merging of small pores into larger ones and by thickening of the pore walls and partitions [48].

In the reference samples and samples with BA10 and BA20 and fired at 1000 °C, slit pores are formed. An increase in porosity is observed in samples BA30 and BA40. This temperature range is characterized by three pore sizes: 1.5 nm, 1.8 nm, and 2 nm. A pore size of 1.5 nm is typical for reference samples and BA10 and BA20 samples. The pore size of 1.8 nm refers to the BA30 samples, the predominance of pores with a diameter of 2 nm is characteristic of samples with the BA40. The shape of slit and cylindrical pores can explain this: the cylindrical pores are isolated and are typical of the material, which is used as an additive; the slit porosity of the samples is interconnected with clay. The BA contains minerals that enter into thermo-chemical transformations resulting in the release of gaseous components (CO_2, H_2) in crystalline water and, as a result, lead to the formation of pores.

4. Conclusions

The bottom ash, formed in incinerating MSW in the CPP, belongs to non-hazardous waste and can be used as an additive in clay bricks production. There are clays with a high CaO content (2.71%) in Lithuania, making it impossible to use additives with a high CaO content. In the presented experimental study, clay raw materials with a low CaO content (0.2%). It has been established that BA particles stabilise shrinkage during drying and reduce shrinkage during firing. The shrinkage is within the acceptable range. The burnout of the small residual amount of organic substances in the clay, the decomposition of calcium carbonate, and the release of gaseous substances and crystalline water during firing lead to a change in the microstructure of clay samples. The result of these transformations is the formation of open porosity and a change in the shape of the pores, leading to a change in the samples' physical

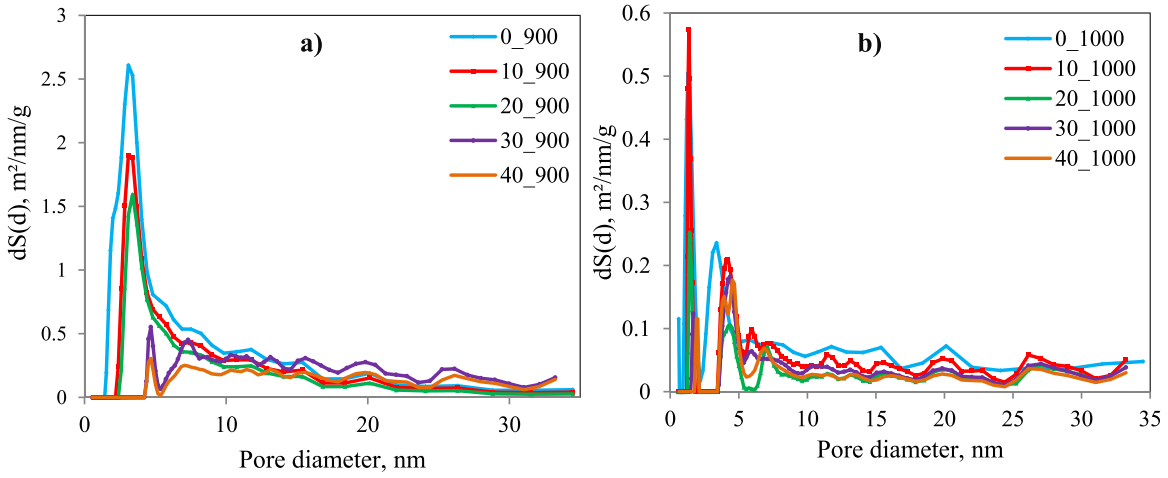

Fig. 14. Pore size distribution from nitrogen adsorption test: a — fired samples at 900 °C; b — fired samples at 1000 °C.

Table 6
N_2 adsorption measurements for clay samples at different firing temperature and amount of BA (DFT method).

Parameters	Temperature firing 900 °C					Temperature firing 1000 °C				
	Amount BA, %									
	0	10	20	30	40	0	10	20	30	40
Specific surface area, m^2/g	11.444	7.923	6.311	6.478	4.513	1.992	1.592	1.122	1.123	0.930
Total pore volume, cc/g	0.051	0.038	0.030	0.027	0.019	0.017	0.006	0.004	0.004	0.003
Pore diameter, nm	3.385	3.385	3.385	26.12	33.24	36.00	33.24	33.24	33.24	33.24

and mechanical properties, frost resistance, and mineralogical composition.

The infrared spectra of clay, BA and clay brick samples fired at 900 and 1000 °C showed the presence of hydroxyl groups (OH) in clay, a small amount of adsorbed water in clay and BA, the C-O bond, which corroborated the presence of $CaCO_3$ in BA and Si-O, Si-O-Mg, Si-O-Al and Al-OH-Al bond for clay, BA and clay brick samples. These results are consistent with the XRD analysis.

Clay bricks containing 10–20% BA and fired at 900 °C had density of 1.93 and 1.92 g/cm^3, shrinkage of approximately 5.9% and 5.5%, the compressive strength of 22.6 and 17 MPa, water absorption of 14% and 14.2%, open porosity is 27.3% and 28.4%, and frost resistance 23 cycles. Frost resistance was determined by repeated freezing and thawing. The clay bricks fired at 1000 °C and containing 10–30% BA had a density approximately of 1.92–1.99 g/cm^3; shrinkage of 6.6–5.8%, compressive strength of 14.5–22.6 MPa, water absorption of 11.7–13.1%, the total open porosity of 25–26%, and frost resistance 25 cycles.

The samples fired at 900 °C and containing 10–20% BA predominated slit pores with a size of 3.3 nm. The clay body samples containing 10–20% BA and fired at 1000 °C had slit pores with a pore diameter of 1.5 nm, but clay brick samples containing 30% BA and fired at the same temperature predominated slit cylindrical pores with a pore diameter of 1.8 nm.

According to LST EN 772–22:2019, clay bricks containing up to 10–20% of BA and fired at 900 and 1000 °C can be utilized in moderately aggressive environments (F1 class). However, specimens containing 30% BA and fired at 1000 °C can be used in passively aggressive environments. Samples can be used for internal use; if used externally bricks are liable to be damaged by frost action if not protected by impermeable cladding or render (F0 class).

According to the results of the thermal conductivity analysis, it was found that the thermal conductivity values directly depend on the porosity of the samples. The values of the measured thermal conductivity for the samples were in the range from 0.49 W to 1.1 W/m·K. In accordance with ASTM D 78896, it can be argued that the addition of bottom ash during clay brick production does not impair the technical properties of the fired samples.

The results of this study point to the possibility of the development of fired clay bricks using up to 30% replacement of clay with bottom ash. However, such a brick depends on its characteristics, particularly the class of frost resistance. In addition, bottom ash used as an additive will reduce the amount of accumulated waste.

Declaration of Competing Interest

The authors declare that they have no known competing financial interests or personal relationships that could have appeared to influence the work reported in this paper.

Acknowledgements

We acknowledge Marius Praspaliauskas, Senior research associate, Laboratory of Heat-Equipment Research and Testing, Lithuanian Energetic Institute (LEI) to help in preparing materials for the experiment.

We would like to say our great gratitude to the staff of the Centre for Hydrogen Energy Technologies, LEI to help with research.

We acknowledge the staff of the Kaunas cogeneration power plant for helping in providing material for research and informational support.

References

[1] M.H. Abdullah, A.S. A. Rashid, U.H. M. Anuar, A. Marto, R. Abuelgasim. Bottom ash utilization: A review on engineering applications and environmental aspects. IOP Conf. Ser.: Mater. Sci. Eng. 527 (2019) 012006, ⟨https://doi:10.1088/1757–899X/527/1/012006⟩.
[2] D. Blasenbauer, F. Huber, J. Lederer, M.J. Quina, D. Blanc-Biscarat, A. Bogush, E. Bontempi, J. Blondeau, J.M. Chimenos, H. Dahlbo, Legal situation and current practice of waste incineration bottom ash utilization in Europe (https://doi), Waste Manag 102 (2020) 868–883, https://doi.org/10.1016/j.wasman.2019.11.031.
[3] Vilnius cogeneration power plant ⟨https://vkj.lt/en/about-us/eu-funding/147⟩.
[4] Kaunas cogeneration power plant ⟨https://kkj.lt/en/about-us/power-plant/93⟩.
[5] Klaipeda cogeneration power plant ⟨https://gren.com/lt/⟩.
[6] B.H. Cho, B.H. Nam, J. An, H. Youn, Municipal solid waste incineration (MSWI) ashes as construction materials-A review (https://doi), Materials 13 (14) (2020) 3143, https://doi.org/10.3390/ma13143143.
[7] R. Taurino, E. Karamanova, L. Barbieri, S. Atanasova-Vladimirova, F. Andreola, A. Karamanov, New fired bricks based on municipal solid waste incinerator bottom ash (https://doi), Waste Manag. Res. (2017) 1–9, https://doi.org/10.1177/0734242×17721343.
[8] A.M. Saleh, M.N. Rahmat, Potential use of municipal solid waste ash (MSWA) as sustainable construction bricks (https://doi), Mater. Sci. Eng. 620 (2019), 012073, https://doi.org/10.1088/1757-899X/620/1/012073.
[9] F.A.M. Lino, K.A.R. Ismail, Recycling and thermal treatment of MSW in a developing country, IOSR J. Eng. 7 (7) (2017) 30–38.

[10] A. Maldonado-Alameda, J. Giro-Paloma, A. Alfocea-Roig, J. Formosa, J. Maria Chimenos, Municipal solid waste incineration bottom ash as sole precursor in the alkali-activated binder formulation (https://doi), Appl. Sci. 10 (2020) 4129, https://doi.org/10.3390/app10124129.
[11] D. Fernández-González, I. Ruiz-Bustinza, J. Mochón, C. González-Gasca, L.F. Verdeja, Iron ore sintering: process, Miner. Process. Extr. Metall. Rev. 38 (2017) 215–227, https://doi.org/10.1080/08827508.2017.1288115.
[12] Y. Xiao, M. Yunusa, D. Jelagin, H. Tan, B. Strnadel, Special Issue on Silicate Solid Waste Recycling, in: Materials, 14, Basel, 2021, p. 3776, https://doi.org/10.3390/ma14143776.
[13] X. Dou, F. Ren, M. Quan Nguyen, A. Ahamed, K. Yin, W. Ping Chan, V. Wei-Chung Chang, Review of MSWI bottom ash utilization from perspectives of collective characterization, treatment and existing application, Renew. Sustain. Energy Rev. 79 (2017) 24–38, https://doi.org/10.1016/j.rser.2017.05.044.
[14] B. Hooi Cho, B. Hyun Nam, J. An, H. Youn, Municipal solid waste incineration (MSWI) ashes as construction materials-A review (https://doi), Materials 13 (2020) 3143, https://doi.org/10.3390/ma13143143.
[15] M. Van Praagh, M. Johansson, J. Fagerqvist, R. Grönholm, N. Hansson, H. Svensson, Recycling of MSWI-bottom ash in paved constructions in Sweden–A risk assessment, Waste Manag 79 (2018) 428–434, https://doi.org/10.1016/j.wasman.2018.07.025.
[16] L.A. Sormunen, P. Kolisoja, Construction of an interim storage field using recovered municipal solid waste incineration bottom ash: Field performance study, Waste Manag 64 (2017) 107–116. ⟨https://urn.fi/URN:ISBN:978-952-15-4019-6⟩.
[17] ⟨https://www.vesco.com.ua/media/brochure-ru.pdf⟩.
[18] L.F. Dutra, M.E. Freitas, A.-C. Grillet, N. Mendes, M. Woloszyn, Microstructural characterization of porous clay-based ceramic composites (https://doi), Materials 12 (2019) 946, https://doi.org/10.3390/ma12060946.
[19] U. Kuila, M. Prasad, Specific surface area and pore-size distribution in clays and shales. European Association of Geoscientists & Engineers, Geophys. Prospect. 61 (2013) 341–362, https://doi.org/10.1111/1365-2478.12028.
[20] A.I. Gusev. Nanomaterials, nanostructures, nanotechnologies. Moskow: Fizmatlit (2005) 416.
[21] M. Thommes, Physical adsorption characterization of nanoporous materials, Chem. Ing. Tech. 82 (2010) 1059–1073, https://doi.org/10.1002/cite.201000064.
[22] N.N. Greenwood, A. Earnshaw (1997) Chemistry of the Elements, second edition. School of chemistry, University of Leeds, U.K. 357 p.
[23] ⟨https://portalkeramiki.ru/index.php/eshop/materials/chemisrtry/59/s-4530-detail⟩.
[24] 2014/955/EU: Commission Decision of 18 December 2014 amending Decision 2000/532/EC on the list of waste pursuant to Directive 2008/98/EC of the European Parliament and of the Council Text with EEA relevance.
[25] J.C.T. Rezende1, V.H.S. Ramos, H.A. Oliveira, R.M.P.B. Oliveira, E. Jesus, Removal of Cr(VI) from aqueous solutions using clay from calumbi geological formation, N. Sra. Socorro, SE State, Brazil, Mater. Sci. Forum 912 (2018) 1–6, https://doi.org/10.4028/www.scientific.net/MSF.912.1.
[26] M.S. Conconi, M. Morosi, J. Maggi, P.E. Zalba, F. Cravero, N.M. Rendtorff, Thermal behavior (TG-DTA-TMA), sintering and properties of a kaolinitic clay from Buenos Aires Province, Argentina, Cerâmica 65 (2019) 227–235, https://doi.org/10.1590/0366-69132019653742621.
[27] H.B. Hadjltaiefa, S.B. Ameurb, P.D. Costac, M.B. Zinaa, M.E. Galvez, Photocatalytic decolorization of cationic and anionic dyes over ZnO nanoparticle immobilized on natural Tunisian clay, Appl. Clay Sci. (2017), https://doi.org/10.1016/j.clay.2017.11.008.
[28] I. Aliu, Comparative analysis of the compressive strengths of clay and sandcrete blocks for low cost housing, J. Eng. Archit. 4 (2) (2021) 19.
[29] ⟨https://www.gobrick.com/docs/default-source/read-research-documents/technicalnotes/9a-specifications-for-and-classification-of-brick.pdf/⟩.
[30] M. Sutcu, E. Erdogmus, O. Gencel, A. Gholampour, E. Atan, T. Ozbakkaloglu, Recycling of bottom ash and fly ash wastes in eco-friendly clay brick production, J. Clean. Prod. 233 (2019) 753–764, https://doi.org/10.1016/j.jclepro.2019.06.017.
[31] O. Kizinievič, V. Voišnienė, V. Kizinievič, I. Pundienė, Impact of municipal solid waste incineration bottom ash on the properties and frost resistance of clay bricks, J. Mater. Cycles Waste Manag. 24 (2022) 237–249, https://doi.org/10.1007/s10163-021-01314-4.
[32] S. Louati, S. Baklouti, B. Samet, Geopolymers base don phosphoric acidand illito-kaolinitic clay, Adv. Mater. Sci. Eng. 7 (2016) 1–7, https://doi.org/10.1155/2016/2359759.
[33] J. Götze, Y. Pan, A. Müller, Mineralogy and mineral chemistry of quartz: a review, Mineral. Mag. 85 (5) (2021) 639–664, https://doi.org/10.1180/mgm.2021.72.
[34] N. Kumari, C. Mohan Basics of Clay Minerals and Their Characteristic Properties. (2021) 1–29, ⟨https://doi:10.5772/intechopen.97672⟩.
[35] Illite mineral data Available from ⟨http://webmineral.com/data/Illite.shtml⟩#.XyAKkJ4zZPY, (Acces.: 2020–08-29).
[36] R. Schoonheydt, C.T. Johnston, F. Bergaya, Surface and interface chemistry of clay minerals 9 (2018) 1–410.
[37] J.-C. Boulliard, E. Gaillou, Twinning in anorthoclase megacrysts from phonolitic eruptions, Erebus volcano, Antarctica (https://doi), Eur. J. Mineral., Copernic. 31 (1) (2019) 99–110, https://doi.org/10.1127/ejm/2019/0031-2804.
[38] S.K. Haldar, J. Tišljar, Introduction to mineralogy and petrology, Chapter 2. Basic Mineral. (2014) 39–79, https://doi.org/10.1016/B978-0-12-408133-8.00002-X.
[39] Ma del Carmen Gutiérrez-Castorena, Interpretation of micromorphological features of soils and regoliths (secondedition), Chapter 6 – Pedogenic Siliceous Features (2018) 127–155, https://doi.org/10.1016/B978-0-444-63522-8.00006-1.
[40] Wollastonite mineral data available from ⟨https://www.ima-na.org/page/what_is_wollastonite⟩.
[41] Y. Lu, Y. Wang, Y. Zhao, Z. Wei, Y. Li, W. Hao, Y. Zhang, The characteristics of mineralogy, morphology and sintering during co-combustion of Zhundong coal and oil shale, RSC Adv. 7 (2017) 51036–51045, https://doi.org/10.1039/C7RA10340A.
[42] J. Kotowski, K. Nejbert, D. Olszewska-Nejbert, Rutile mineral chemistry and Zr-in-rutile thermometry in provenance study of Albian (Uppermost Lower Cretaceous) terrigenous quartz sands and sandstones in southern extra-carpathian Poland, Miner 11 (2021) 553, https://doi.org/10.3390/min11060553.
[43] M. Muhammad, A. Fatmaliana, Z. Jalil. Study of hematite mineral (Fe2O3) extracted from natural iron ore prepared by co-precipitation method, IOP Conference Series: Earth and Environmental Science (2019) 348 012135.
[44] Labrodarite mineral data available from ⟨https://www.mindat.org/min-2308.html⟩.
[45] Diopside mineral data available from ⟨https://www.mindat.org/min-1294.html⟩.
[46] T. Safonova, Y. Zykova, Malacolite- an efficient admixture in brick production, Bull. Irkutsk State Tech. Univ. 3 (39) (2009) 174–180.
[47] A. Alothman, Z.A Review: Fundamental aspects of silicate mesoporous materials, Materials 5 (12) (2012) 2874–2902, https://doi.org/10.3390/ma5122874.
[48] N. Grubeša, M. Vračević, J. Ranogajec, V. Vučetić, Influence of pore-size distribution on the resistance of clay brick to freeze-thaw cycles, Materials 13 (10) (2020) 2364, https://doi.org/10.3390/ma13102364.